# Spectrometric Response of Large Volume CdZnTe Coplanar Detectors

Raquel González , José M. Pérez, Oscar Vela, Eduardo de Burgos, Juan C. Oller and Vladimir Gostilo

***Abstract*—In this paper the spectroscopic performance of a new large volume coplanar detector is studied. Spectrometric results using classical techniques are presented. The new unit confirmed that this design of coplanar-grid anodes provided an acceptable balance between anode weighting potentials. The material of this detector is not as homogeneous as desirable. Nonetheless, the detector demonstrated a resolution of the order of 2.7% FWHM for 662 keV. The spectroscopic properties at different interaction depths were studied by making use of a multi-parametric digital system. Depth sensing achievable resolution is quantified by making use of this setup. The interaction profile at different depths of the detector was compared with that expected in ideal detectors. An adaptation of the multi-parametric digital system was applied to the study of the waveforms generated in the preamplifiers connected to the electrodes. Induced charge waveforms at selected interaction depths were analyzed in order to study the deviations in the interaction depth profiles found between simulation and theory. The causes are attributed to trapping effects in the detector bulk. Unexpected pulses are explained by modeling the charge drift in the detector. The mobility of electrons in these detectors was studied by digital signal analysis, which gave a value close to 950 $cm^2V^{-1}s^{-1}$ at room temperature. Results of the dependence of $\mu_e$ with *T* are presented in the operation temperature range of these detectors.**

## I. Introduction

THE concept of coplanar-grid anodes was first applied to CdZnTe crystals by 1995 [1,2], as a method to overcome the intrinsic limitation of the deficient hole transport in gamma radiation detectors based on this type of semiconductor. In these detectors, the difference of the two signals induced in the coplanar anodes by the radiation practically depends solely on the transport of the electrons created by the radiation in the bulk. In most of the detector volume there is no hole dependency of the induced signal. The sensor, therefore, becomes a unipolar device. By making use of the differential anode gain technique [2], effects of electron trapping in the bulk could be compensated for and large volume units demonstrated acceptable values of energy resolution. Given the results achieved with large volume detectors and the simplicity of the analog front end electronics needed to operate them, an interest in coplanar-grid detectors for practical applications is emerging [3]. On the other hand, by combining the signal induced in coplanar anodes and planar cathode, coplanar-grid detectors enabled the implementation of techniques to estimate the effective interaction depth of the gamma photons in the bulk [4]. This technique was also shown to be effective for spectrometry with other type of detectors, such as strip [5] or pixel [6] arrays.

Once the coplanar technique was confirmed to be operative for constructing large volume CdZnTe detectors, our efforts were focused on the design of new anode patterns to improve the spectrometric response. The correct balancing of the weighting potentials associated with the collecting and non-collecting anodes provided promising expectations [7], and subsequently confirmed [8]. In a recent work [9], the last generation of a series of designs were shown to reach an acceptable balance between anodes. It was experimentally demonstrated that in coplanar-grid detectors with generation IV anode pattern, the spectroscopic resolution does not depend on the interaction depth.

In this paper we describe the spectroscopic performance of a second coplanar-grid detector with generation IV anode pattern, manufactured by BSI with a crystal grown by eV Products. While the unit studied in [9] used a circular pattern, the unit in the detector presented in this paper is rectangular. Spectrometric results using classical techniques are also presented. The spectroscopic properties at different interaction depths were studied by making use of a multi-parametric digital system. The absolute resolution in the location of the interaction depth was measured. Errors in the estimate of this parameter are analyzed, together with some possible causes of these errors.

An adaptation of the multi-parametric digital system is applied to the study of the waveforms generated in the

Manuscript received October 28, 2004. This work was supported by the Spanish Ministry of Education under Grant ref. TIC2002-02367.

R. González is with CIEMAT, Lab. de Electrónica y Automática CIEMAT. Edificio 22. Avda Complutense, 22, E-28040 Madrid. SPAIN (telephone: +34 91 346 6845, e-mail: raquel.gonzalez @ciemat.es).

J. M. Pérez is with CIEMAT, Lab. de Electrónica y Automática CIEMAT. Edificio 22. Avda Complutense, 22, E-28040 Madrid. SPAIN (telephone: +34 91 346 6557, e-mail: jm.perez @ciemat.es).

O. Vela is with CIEMAT, Lab. de Electrónica y Automática CIEMAT. Edificio 22. Avda Complutense, 22, E-28040 Madrid. SPAIN (telephone: +34 91 346 6024, e-mail: oscar.vela @ciemat.es).

E. de Burgos is with CIEMAT, Lab. de Electrónica y Automática, CIEMAT. Edificio 22. Avda Complutense, 22, E-28040 Madrid. SPAIN (telephone: +34 91 346 6728, e-mail: Eduardo.burgos @ciemat.es).

J. C. Oller is with CIEMAT, Lab. de Electrónica y Automática CIEMAT. Edificio 22. Avda Complutense, 22, E-28040 Madrid. SPAIN (telephone: +34 91 346 6033, e-mail: jc.oller @ciemat.es).

V. Gostillo is with BSI, Ganibu Dambis 26, P.O.Box 33, Riga, LV-1005, LATVIA. (telephone: +371 7383947, e-mail: bsi@bsi.lv.)

preamplifiers connected to electrodes. In this way, the pulses induced by radiation in the anodes and cathode can be digitized and studied. Experimental unexpected pulses were analyzed and explained within the framework of the electric field profile modeled for an ideal detector with this anode pattern. The detector characterization is completed with the study of the mobility of electrons in the bulk.

## II. Detector Construction and Analog Characterization

### A. Detector Manufacturing

Detector M0904 was constructed by BSI, Latvia starting with eV-Products material. The crystal was received from eV-Products as planar detector (reference M09-619222-04) with platinum contacts. Its dimensions were 1.5 cm × 1.5 cm × 1.0 cm. The detector edges showed "drops" as a result of the etching processes. The surface had small bumps, which corresponded to external structural defects, and roughness. Traces of cutting by disc saw were visible. The detector presented a cavity at one of two metallized faces, in the center of which were seen as a presence of structural heterogeneities.

Registered spectra irradiating the planar detector from the cathode side with alpha particles presented false double peak at low voltages (<100 V), which is evidence of detector heterogeneities. Pulse shapes showed heterogeneous charge carrier transport. This can be related to non-uniformities in the electric field distribution or electro-physical characteristics (mobility and life time) within the detector volume.

The planar electrodes were removed and new electrode patterns were deposited by gold evaporation through masks. In the anode face, the pattern corresponding to generation IV with rectangular symmetry was used (see Fig. 1). The crystal was mounted on a $Al_2O_3$ substrate and the electrodes wire-bonded with gold wire to the contact pins. The substrate was placed in a metal aluminum case with a beryllium entrance window in front of the cathode. The volume inside the case was filled with sorbent. The leakage current between the grids at 50 V was 149.7 nA what provides a resistance between the grids of 0.33 GΩ at this voltage.

This is the second generation IV design we tested in our laboratory. The first one [9] used a circular pattern. There is a reason for this new design. We were interested in checking for possible differences between cylindrical and rectangular symmetries. The designs of the anode pattern are mainly related to the definition of strip widths and distance between strips, but each symmetry provides some extra advantages and disadvantages to the design. For example, the circular design leads to longer strips on each anode, which is a technological disadvantage. Another disadvantage of the circular design is that in the central region of the detector the two anode weighting potentials are not properly balanced. On the other hand, there are no sharp corners on this symmetry, which is a significant potential advantage.

### B. Spectrometric Response

The analog front end electronics used in this work was based in two A250 preamplifiers from Amptek with the 2SK152 input FET, also provided by Amptek, AC coupled to the anode connections. The preamplifiers were mounted on PCA250 circuit boards. The output of the preamplifiers were connected to a subtraction circuit with adjustable relative gain. The subtraction circuit was made by making use of a CLC409 operational amplifier, mounted on a custom board. In order to obtain information regarding the photon interaction depth, the cathode signal was read out by a third A250 preamplifier mounted in AC configuration. Therefore, the front-end analog electronics delivers the following output signals: collecting anode direct output, non-collecting anode direct output, subtracted anode signal and cathode output. Four Ortec 885 gaussian shaper amplifiers with time constant set to 1.5 μs and a precision test pulse generator Ortec 204 completed the analog setup. Without connecting the detector, the intrinsic electronic noise for the complete direct anodes and cathode outputs were 175 e- rms (~2 keV FWHM CZT). The intrinsic noise in the subtraction circuit, without connecting the detector, was 260 e- rms (~ 3 keV FWHM CZT). The electronic noise with the detector connected and biased (-1,200 V cathode bias, 30 V differential anode bias) was, in the worst case, 655e- rms for the subtraction circuit and 405e- rms for the cathode channel.

Spectroscopic performance of the unit was tested by considering the differential anode gain technique [2]. Cathode bias was ranged from −500 V to −1,500 V. The differential voltage between anodes was tested from 10 V to 50 V. The optimal operation conditions were −1,200 V cathode bias, 30 V differential anode bias. The guard ring was grounded in all the measurements performed in this work. Fig. 2 shows a typical spectrum acquired with a $^{137}Cs$ source and the setup described above. The peak at 500 keV corresponded to the pulser test peak. A resolution in the order of 2.7% at 662 keV is nominally obtained. The non-homogeneity of the detector crystal mentioned above contributed to the deviation from the value obtained with similar detectors in the past (~2.2 %).

## III. Multiparametric Study

### A. The Multiparametric Analyzer Setup

It is well known that the interaction depth of each detected event can be estimated in coplanar-grid detectors [7]. This is a valuable technique to evaluate the performance of different regions of the detector. For example, differences in the spectroscopic performance of the detector slices close to anode and cathode surfaces can be used to evaluate the balancing of two anode weighting potentials [7]. A multiparametric acquisition system was constructed to check the spectrometric performance of the detector at different interaction depths. Two Gage CompuScope 12100 PCI boards provided four

digitization channels with a resolution of 12 bits and 50 MS/s sampling rate. Digitizers were programmed with a code written in LabWindows (National Instruments). The code was designed as a multi-purpose data acquisition system, optimized for our detectors. In the multichannel model, the signals generated by the gaussian shapers connected to the anode subtraction circuit and the cathode output were digitized. The system is triggered by a reference amplitude level, using the differential anode signal channel as trigger source. When a pulse is detected, gaussian pulse waveforms are acquired in parallel by the cathode and differential anode channels. Their two maximum absolute amplitudes are calculated and processed. The ratio $R$ between the maximum cathode amplitude and differential anode amplitude is used as an estimate of the interaction depth [9]. According to $R$, the total detector depth is split in a number of divisions $N_Z$. For each interaction, the amplitude of the total induced charge is provided by the maximum amplitude in the differential anode channel. $N_Z$ pulse height histograms are stored, one per depth division, operating as a multiparametric multichannel analyzer.

In the analysis of the interaction depth, the gains of the two electronic channels involved are critical. The differential anode and cathode gains must be identical. In this way, gains of collecting anode, non-collecting anode and cathode were characterized in detail. The variable resistor in the subtraction circuit feedback was tuned by making use of the test pulser connected to the anode preamplifiers, this channel providing the same absolute amplitude for the test signal connected to either anode input. After the anode amplitude adjustment, cathode channel gain was set to be identical to the one provided by the anodes by modifying the fine gain control of its gaussian shaper amplifier module. The measurements of amplitude in the analog channels were performed in a digital oscilloscope. According to the measured resolution and the experimental uncertainty in the control of the gains, an error lower than 2% can be expected in the gain adjustments.

For the calibration of the analog channel gains described above, the capacitors in the test input channel of the PCA250 preamplification boards were considered to be identical (2 pF). Nonetheless, their values can fluctuate. To overcome (at least partially) this uncertainty, a second adjustment in the cathode-anode gains were performed by making use of a gamma source. The spectra for a $^{137}$Cs source acquired in the same experimental conditions by the collecting anode channel and the cathode were compared. The cathode gain was slightly modified until the maximum energy in the two spectra coincided; see Fig. 3.

### *B. Calibration of Proper Resolution*

The resolution in the calculation of the parameter $R$ depends on several factors. The first of them is the fluctuation in the computing of anode and cathode amplitudes due to electronic noise in the detector-preamplifier-amplifier channel. We estimated the influence of these fluctuations in the depth sensing resolution for the experimental configuration used in this paper. The test pulser was connected in parallel to the collecting anode and cathode preamplifier test input, and the parameter $R$ was calculated following the procedures described previously. In order to provide an accurate estimate of the depth resolution, a very large value for $N_Z$ was considered, compared with the depth resolution qualitatively deducted in other works. In these measurements, the detector was connected to the preamplifiers and high voltage applied. Fig. 4 presents the interaction depth results, together with the fit to a gaussian curve for a test pulse amplitude equivalent to 524 keV. The resolution estimated, in terms of full width at half maximum, was ~0.05; this corresponds to one part in 20. According to this result, an acceptable value for $N_Z$ will be 20, corresponding to a precision of 0.5 mm in a 10 mm thick detector.

As confirmation, the detector was irradiated with a $^{90}$Sr beta source (energy range equal to 2,281 keV). The energy of the emitted electrons is sufficiently high to enable the electrons to pass through the beryllium layer, but stopped in the CdZnTe crystal, close to the cathode surface. A simulation was performed in order to estimate the range of the 90Sr electrons in the detector. A modification of the code based on Geant4 presented in [9] was used. The new detector was modeled in its experimental setup, defining precisely the beryllium entrance window and detector-source geometry. The distribution function for the energy emission was approached to a simplification of that collected with 0.5cm thick silicon surface-barrier detectors for 90Sr-90Y source [10]. For $N_Z$ = 20, i.e., 20 divisions of 0.05 cm thick each of them, more than 95% of the electrons are stopped in the first division closer to the cathode. Around 2% of the total events are stopped in the second one. Results of the calculated depth profile is presented in Fig. 5 for $N_Z$ = 20. This figure supports the results obtained previously for depth resolution.

### *C. Results*

The generation IV anode pattern was shown to provide a good balance between collecting and non-collecting anode weighting potentials [9]. This result is confirmed in this work. The spectrometric response at two representative interaction depths are shown in Fig. 6. A $^{137}$Cs point source irradiated the cathode face without using collimation. $N_Z$ was set to 20 in this experiment. The energy resolution for the photopeak in the spectrum shown in Fig 6 acquired close to the anode face is 2.5 % FWHM, a better result than the one achieved in the region close to the cathode face. This is an important result. In this detector, the resolution worsening due to differences between the weighting potentials of the two anodes was less relevant than the resolution worsening due to non-ideal transport properties in the crystal; the spectrum in the anode side is not sensitive to the defects in the crystal, whereas the spectrum near the cathode is. As a consequence, it can be

inferred that better spectrometric results can be achieved with this anode pattern using a higher quality crystal.

The detector efficiency was experimentally studied in this unit. The results obtained with this detector are shown in Fig. 7.a for total efficiency and 7.b for photopeak efficiency. Reported values in Fig. 7 are relative to the total acquired events. A $^{137}$Cs point source located just in the center of the detector, at 15 mm from the cathode surface, was used to generate the data shown in this figure. In a previous work [9] the interaction depth on an ideal detector irradiated with 662 keV photons was simulated, using a simulated setup similar to the one in the experiment. The results for simulated for total efficiency (Fig. 9.a of [9]) and photopeak efficiency (Fig. 9.b of [9]) were reported. Comparing Fig. 7.a and 7.b with the simulated curves in Fig. 9.a. and 9.b of [9], a general agreement was found between them. The efficiency profiles obtained follow the expected theoretical distribution in an ideal device. But apart from this general results, a difference between experiment and theory was found: both in Fig 7.a. and 7.b, some events are located at interaction depths larger than 1.0, in percentages than cannot be considered as negligible. $R$ is larger that 1.1 in more than 6% of the total acquired events. According to the resolution in the estimate of the interaction depth, this deviation cannot be attributed to uncertainties in the resolution. Three possible causes are given to explain this effect:

1. Differences in the anodes and cathode channel gains
2. Interactions at the detector edges
3. Trapping effects.

As described in III.*A*, a lot of effort was made in this work to avoid significant differences in the gains of the three analog channels. Therefore, item 1 above should be disregarded. In this detector, if the charge is partially collected by the guard-ring, the pulse induced in the collecting anode should be proportionally lower than expected. If the interaction occurred in a position far from the anode surface, the total amplitude of the pulse induced in the cathode could be larger than the one provided by the subtraction of collecting and non-collecting anode. Although the statistics of the problem reported above seems to be very large to be explained just by this cause, this hypothesis is possible, and item 2 must be considered further.

If the charge induced by the radiation is trapped abruptly in a trapping center near the anode surface, the total charge induced in the anodes should be lower than the one induced in the cathode. Although less intuitive, this significant reduction of total charge induced in the anodes, compared with the one in the cathode, is also possible for uniform trapping in the bulk.

The possible causes presented as an explanation for this effect cannot be analyzed with the digitization system described in this section. The gaussian filter is excellent for increasing the signal to noise ratio, but distort the shape of the induced charge waveforms. A possible way to study the effects mentioned in items 2 and 3 above is to digitize the pulses generated by the preamplifiers before being filtered with the shapers. The input range of the digitizing boards used in this work does not enable an analysis of the signal generated by the preamplifiers. A new digitization system was constructed by making use of a digital oscilloscope whose input voltage range is compatible with the amplitude of the pulses generated at the output of the preamplifiers. With this new system, item 3 was addressed. Because of limitations in the experimental setup, we leave the study of the effects of detector edges for another work.

## IV. Digital Analysis of Waveforms

### *A. The Waveform Analyzer*

A version of the software written for the multi-parametric MCA developed with the Gage CompuScope digitizing boards was implemented in the control computer of a Tektronics digital oscilloscope model TDS 5054 (8 bits vertical resolution, band 500 MHz, sampling rate 5 GS/s). In this version, the input signals were the 50Ω outputs provided by the A250 preamplifiers and the subtraction circuit. The gaussian shapers were not used. Pulses were acquired in coincidence from four channels, namely: the subtraction circuit with differential gain set exactly to 1.0 (channel 1), cathode preamplifier output (channel 2), collecting anode (channel 3) and non-collecting anode (channel 4). The system was triggered from channel 1, by using a standard level trigger. For each acquisition, the maximum amplitudes of differential anode and cathode signals were computed in the following way. Each pulse acquisition was made up of 2,500 samples. The trigger horizontal position was set to 1/3 of the pulse width. The last 500 samples were used to estimate the maximum amplitude of the pulse. This value minus the reference position for the base line was the estimate of the total pulse amplitude. Both anode and cathode signals was sufficiently stable for this algorithm to work properly.

By using channels 1 and 2, the system worked as a version of the multiparametric multichannel analyzer, enabling it to compute the interaction depth of the event. The resolution of this system was poorer than the one implemented with the digitizers, because of the lower signal to noise ratio of the input signals and the lower vertical resolution of the oscilloscope. Spectra were acquired with both equipments under the same conditions using a test pulser, in order to provide a comparison of the energy resolution. While the resolution obtained with the multi-parametric analyzer constructed with the digitizers was 1.37 % for an equivalent energy of 527 keV, the resolution with the oscilloscope was 2.37%. In spite of these limitation, the system could be used for depth sensing studies, with the depth resolution decreased by a factor of 1.5 when compared with the results for the digitizers in Fig. 4. The maximum effective value for $N_Z$ in this system is 14, corresponding to a depth resolution of 0.72 mm in the detector. Furthermore, the system was programmed to

acquire in parallel waveforms from the three channels of interest. In this way, we could select and store waveforms from anodes and cathode corresponding to selected interaction depths.

### B. Experimental Results

With the digitizer implemented in the oscilloscope we were able to confirm events with interaction depth estimates larger than 1.0. The central part of the detector cathode surface was irradiated with the $^{90}$Sr radioactive source, avoiding the detector areas near the cathode borders. The detector depth was divided into 20 slices ($N_Z$ set to 20). In order to analyze the source of this problem, the interaction depth was studied from $R$=0.0 to $R$=2.0, i.e., 20 real divisions of the detector were surveyed, plus another non-real 20 divisions. Practically all the pulses analyzed above the slice 20 (interaction depths larger than 1.0) had shapes as shown in Fig. 8.

Two main types of waveforms were identified in these undesired depth values: pulses with uniform slopes during the charge drift throughout the bulk (see Fig. 8.a and 8.b) and pulses with evidences of non-uniformities (Fig. 8.c and 8.d). These last group of pulses corresponded to events in which the drift towards the anodes of electrons produced by the radiation was affected by non-uniformities in the electrical parameters (mobility, trapping time or electric field) of the detector. Pulses with uniform slopes and anode deficit can be due to uniform trapping effects.

### C. Theoretical Confirmation

As a confirmation that charge trapping can explain the error in the interaction depth estimate, the drift of the charge was simulated in the detector for different values of trapping. The electric field in the M0904 detector was modeled by making use of ANSYS 6.0, and using a 3D model. The drift of the charge in the detector was simulated in discrete time steps of $10^{-8}$ s. At each step, by knowing the previous position $\vec{r}(t)$, the next position is computed by assuming the following relationship:

$$\vec{r}(t+\Delta t) = \vec{r}(t) + \mu \vec{E}(t)\cdot\Delta t \ , \qquad (1)$$

where $\mu$ is the electron mobility in the CdZnTe detectors and $\vec{E}(t)$ the electric field at the position $\vec{r}(t)$. The mobility is assumed to be constant. The value of 1,000 $cm^2V^{-1}s^{-1}$ was used (see Section V). The electric field value at each $\vec{r}(t)$ was calculated from the values provided by ANSYS in a grid of positions in the area simulated. Values of cathode and anode biases similar to those used in operation were used (−1200 V cathode, −33 V non-collecting anode, guard-ring grounded). To reduce the complexity of the calculations, only the plane at $Y$=0, the axis perpendicular to the anode strips, of the detector was considered (Fig. 1), whilst assuming a two dimensional model of the detector. The electric field at each position was interpolated from the values in all points of the grid simulated by ANSYS, giving a higher weight to those points of the grid at distance to $\vec{r}(t)$ lower than a pre-selected radius. In this way, the interpolation is more sensitive to local values, and reduces fluctuations between consecutive points. The algorithm used was a variant of the Shepard´s method, similar to the one reported in [11].

Following the procedure described above, paths of charges generated near cathode surface at $X$ positions close to 0.0 were tracked, from the position the charge was generated until it reached the anode surface. Since the weighting potentials associated to the anodes and the cathode at each point of this path can be computed with ANSYS, in a similar way as for the electric field, the induced charge can be obtained by making use of the Shockley-Ramo theorem [12,13]:

$$Q_i(t) = -qN(\vec{r}(t))V_i^0(\vec{r}(t)) \ , \qquad (2)$$

where $N(\vec{r})$ and $V_i^0(\vec{r})$ are the remaining free charge and the extrapolated value of the weighting potential of the electrode $i$ at position $\vec{r}(t)$, respectively. The trapping of the charge was simulated by assuming that at each step the total charge is reduced by:

$$N(\vec{r}(t+\Delta t)) = N(\vec{r}(t))e^{-\Delta t/\tau} \ . \qquad (3)$$

Secondary effects such as diffusion are not considered in this study. Results of the simulation for two cases in which the charges are produced near the cathode surface are shown in Fig. 9. The cathode bias was set to −1,200 V, and non-collecting anode bias to +33V. The initial charge deposited was 1.0 and the electron mobility $\mu_e$ = 1,000 $cm^2V^{-1}s^{-1}$. In Fig. 9.a, the electron trapping time $\tau_e$ was very high, $50\times10^{-6}$ s, and in Fig. 9.b two orders of magnitude lower ($0.5\times10^{-6}$ s.). Fig. 9.b confirms that item 3 in III.*C* can be a cause for the errors found in the interaction depth estimate. We want to point out that the purpose of this comparison is just to provide a possible explanation for the pulses with shapes shown in Fig. 8. At the present level of accuracy of the algorithms used for the generation of the simulation pulses, only a qualitative justification can be provided. Efforts are being made to implement a more realistic electric field in the detector, a more accurate tracking of the induced charge towards the electrode and the inclusion of diffusion.

## V. Transport Parameters

In this and previous studies, the value for the electron mobility in our detectors was assumed to be 1,000 $cm^2V^{-1}s^{-1}$. This is an averaged value found in the literature (see [14] for a compilation of reported values). Many relevant concepts in our simulations and experiments depend on this value. Therefore, this parameter is sufficiently important to be studied experimentally. The setup described in Section IV can be used for this purpose because it was designed to digitize waveforms and provide the interaction depth at the same time. Selecting pulses from photons that deposited their energy far from the

anode surface, the charge induced in the cathode channel can be approximated by the Hecht's relation [14]:

$$Q(t) = \frac{N_0 eE}{d} \mu_e \tau_e (1 - e^{-t/\tau_e}) \ , \qquad (4)$$

for $t$ lower than the maximum collection time. $N_0$ in the equation above represents the total charge deposited by the photon; $e$ is the electron charge, $E$ the electric field, $\mu_e$ the electron mobility and $\tau_e$ the electron trapping time. The parameter $d$ in this detector represents the distance from the interaction point to the detector depth close to the anode face in which the electric field lines are deflected towards the collecting anode. In this region, the electric field rapidly increases, giving a rather short collecting time. The width of this region can be calculated from the waveforms. In this paper, an averaged value of 0.5 mm is considered. Thus, for photons with $R$ close to 1.0, d = 0.95 will be assumed.

In order to fit the experimental value to Hecht's relation, is it more efficient to normalize the induced charge, relative to the total one, namely, $Q_{max} = Q(t=d/(\mu_e E))$:

$$\frac{Q(t)}{Q_{max}} = \frac{1 - e^{-t/\tau_e}}{1 - e^{-d/\mu_e \tau_e E}} \ . \qquad (5)$$

Fig. 10 shows a representative result of a fit to the last equation. The pulse were acquired with detector M0904 irradiated with a $^{137}$Cs source. For a good fit, only very uniform pulses were selected. Cathode bias was –1,200 V and differential anode bias 33 V, guard-ring grounded. The code Origin was used to estimate the free parameters of this equation, $\mu_e$ and $\tau_e$. The values calculated for the pulse shown in Fig. 10 were $\mu_e = 933 \pm 2$ cm$^2$V$^{-1}$s$^{-1}$ and $\tau_e = 1.48\times10^{-6} \pm 5\times10^{-8}$ s (the error values correspond to those obtained in the fit to Hecht´s relation).

A detailed study of the mobility was performed with the detector M02.2-1. The value of this parameter was studied in a short range of temperatures, from +10ºC to +40ºC, the operation temperature range of the detectors. The front-end electronics box was introduced in a climatic chamber that enabled the temperature of the detector to be controlled with a precision better than 0.1ºC. Prior to the measurements at each temperature, the chamber temperature was stabilized for two hours. Waveforms were acquired for the detector irradiated with a $^{137}$Cs radioactive source. Pulses with $R$ close to 1.0 were selected and stored. In order to check the detector at different configurations, pulses were acquired at four different cathode biases at each temperature: –600, –800, –1,000 and –1,200 V. Anode bias was set to +30 V. Results of the fit for a number of pulses at different temperatures are shown in Fig. 11. From Fig. 11, it can be stated that the uncertainty in the estimate of $\mu_e$ is rather significant. Although the error in the depth estimate in the pulses contributes to the uncertainty in the mobility calculation, the main cause of this can be attributed to the non-homogeneities in the detector.

Fig. 12 presents the averaged values at different temperatures, together with the uncertainties in the estimate of the value. For each temperature, results for ~20 pulses were averaged. For each single pulse the uncertainty in the mobility estimate was ~± 2 cm$^2$V$^{-1}$s$^{-1}$. Due to the significant differences in the fit values for each pulses, this uncertainty increases the value, on average, up to between 20 and 30 cm$^2$V$^{-1}$s$^{-1}$ on the average. It is evident that uncertainties are too large to infer a precise trend with temperature. Nonetheless, these data can confirm the trends of the mobility as $T^{-x}$, for $0.5 \le x \le 1.0$. Regarding the experimental data shown in Fig. 12, it must be pointed out that they can also be acceptably fitted by a linear function. We selected a potential law because the extrapolation to lower temperatures of the results provided by the fit to a power law is in better agreement with theoretical trends for CdTe and ZnTe [15] than a linear fit. From the results obtained, we will assume in future works the mobility to vary in this detector with $T^{-0.5}$.

## VI. Conclusions

The new unit M0904 confirmed that this design of coplanar-grid anodes provides an acceptable balance between anode weighting potentials. The material of this detector is not as homogeneous as desirable. Nonetheless, the detector demonstrated a resolution of the order of 2.7% FWHM for 662 keV. This result validates the procedures of BSI for the construction of coplanar-grid detectors and from this it can be inferred that higher resolution can be expected in future units based on better crystals. Regarding the expected differences between the circular and rectangular generation IV patterns, we were unable to find differences related to the detector symmetry, mainly because of non-uniformities in the crystal.

The digitization system that enabled the implementation of a multiparametric multichannel analyzer was extended to other applications. According to our needs, it can be selected either the use of gaussian shaped signal for having good signal to noise ratio, or direct preamplifier outputs for performing studies of depth sensing in parallel with digital analysis of induced charge waveforms. By making use of the first version, the depth sensing resolution was quantified. The interaction profiles at different depths of the detector were compared with the expected in ideal detectors. By studying induced charge waveforms at selected interaction depths, evidences were found to show that the deviations in the interaction depth profiles found between simulation and theory can be due to trapping effects in the detector bulk. Finally, the mobility of electrons in these detectors was studied, giving a value close to 950 cm$^2$V$^{-1}$s$^{-1}$ at room temperature. From the results presented in this work, we will assume that, in the temperature range in which the detectors will be operated (from +10ºC to +50ºC), $\mu_e$ varies with $T$ in the detector M02.1-1 as $T^{-0.5}$. This information is needed in the electrical study of the units carrying out in our laboratories.

Two questions were not addressed in this work. The first one is the contribution of the detector edges to the generation of unexpected pulses. The second question is the implementation of a more realistic simulation of the charge pulses induced by the energy deposited in the detector. As mentioned above, these two points are being addressed and will be the basis of a new publication.

## VII. References


[1] P. N. Luke. "Single-polarity charge sensing in ionizing detectors using coplanar electrodes". *Appl. Phys. Lett*., Vol 65 (22), November 1994, pp. 2884-2886.

[2] P. N. Luke. "Unipolar Charge Sensing with Coplanar Electrodes Application to Semiconductor Detectors". *IEEE Trans. Nucl. Sci*, Vol 42, No 4, August 1995, pp. 207-213.

[3] P.N. Luke, M. Amman, J.S. Lee, B.A. Ludewight, H. Yaver. " A CdZnTe coplanar-grid detector array for environmental remediation." *Nucl. Instrum. Methods*, A 458 (2001), pp. 319-324.

[4] Z. He, G.K. Knoll, D.K. Wehe, J. Miyamoto. "Position sensitive single carrier CdZnTe detectors". *Nucl. Instrum. Methods*, A 388 (1997) pp 180-185.

[5] M.A.J. van Pamelen, C.Budtz-Jorgensen. "Novel electrode geometry to improve performance of CdZnTe detectors". *Nucl. Instrum. Methods*, A 403 (1998) pp 390-398.

[6] Z. He, W. Li, G.K. Knoll, D.K. Wehe, J. Berry, C.M. Stahle. "3-D position sensitive CdZnTe gamma ray detectors". *Nucl. Instrum. Methods*, A 422 (1999) pp 173-178.

[7] Z. He, G.K. Knoll, D.K. Wehe, Y.F. Du. "Coplanar Grid Pattern and their Effect on Energy Resolution of CdZnTe Detectors." *Nucl. Instrum. Methods*, A 411 (1998), pp. 107-113.

[8] J.M. Pérez, Z. He, D. Wehe. "Stability and Characteristics of Large CZT Coplanar Electrode Detectors." *IEEE Trans. Nucl. Sci*, Vol 48, No 3, June 2001, pp. 272-277.

[9] R. González, J.M. Pérez, Z. He. "Efficiency at different interactions depth in large coplanar CdZnTe detector". *Nucl. Instrum. Methods*, A 531 (2004), pp. 544-559.

[10] J.S. Pruitt, C.G. Soares, M. Ehrlich. "Calibration of Beta-Radiation Instruments and Sources". NBS Special Publication 250-21. April 1988. Library of Congress Catalog Card Number 88-600514.

[11] Library E01, Interpolation. NAG Fortran Library Introductory Guide. Mark 20. September 2001.

[12] T.H. Prettyman, K.D. Ianakiev, S.A. Soldner, Cs. Szeles. "Effect of differential bias on the transport of electrons in coplanar grid CdZnTe detectors". *Nucl. Instrum. Methods*, A 476 (2002), pp. 658-664.

[13] Z. He. "Review of the Shockley-Ramo theorem and its application in semiconductor gamma-ray detectors." *Nucl. Instrum. Methods*, A 463 (2001), pp. 250-267.

[14] T.E. Schlesinger, J.E. Toney, H. Yoon, E.Y. Lee, B.A. Brunett, L. Franks, R.B. James. "Cadmium zinc telluride and its use as a nuclear radiation detector material". *Material Science and Engineering*, Vol. 32 (2001), pp 103-189.

[15] J.E. Toney, T.E. Schlesinger, R.B. James. "Optimal bandgap variants of $Cd_{1-x}Zn_xTe$ for high-resolution X-ray and gamma-ray spectroscopy". *Nucl. Instrum. Methods*, A 428 (1999), pp. 14-24.


## VIII. Figure captions

Fig. 1. Schematic representation of the anode pattern implemented in the detector M0904.

Fig. 2. Representative spectrum acquired with detector M0904. The values of the resolution for the 662 keV peak and the test pulser peak at 500 keV are shown.

Fig. 3. Comparison of the spectra obtained from cathode and collecting anode, in identical experimental conditions. The detector was irradiated with a $^{137}$Cs source. Energy channels are not calibrated.

Fig. 4. Interaction depth profile obtained for calibration with the test signal connected in parallel to both cathode and non-collecting anode. For this plot, 80 divisions of the total detector thickness were considered.

Fig. 5. Interaction depth profile obtained by irradiating the detector with a $^{90}$Sr beta source, for $N_Z = 20$.

Fig. 6. Spectrometric response of the detector M0904 at two extreme interaction depths: near the anode surface and near the cathode surface, for 20 divisions of the total detector thickness.

Fig. 7. Detector efficiency obtained at different interaction depth, irradiating with a $^{137}$Cs source. Reported values are relative to the total acquired events at their corresponding ranges. (a) total efficiency, from 90 to 700 keV (b) 662 keV photopeak efficiency.

Fig. 8. Waveforms digitized at the preamplifier outputs of the cathode (light gray), collecting anode (black) and non-collecting anode (dark gray) channels, corresponding to interaction depths larger than 1.0. Differential anode bias was set to 33 V. Cathode bias was set to –1,200 V in (a) and (c). Cathode bias was set to –800 V in (c) and (d).

Fig. 9. Induced charge waveforms simulated for an interaction produced near the cathode surface in a detector with generation IV anode pattern, for the cases of trapping effects negligible (a) and relevant (b).

Fig. 10. Example of the fits to Hecht´s relation carried out in this work. The waveform of the cathode channel (dark gray) is fit to the expression in (5).

Fig. 11. Values of $\mu_e$ calculated for waveforms corresponding to interactions with depth parameter close to 1.0. The $X$ axis represents the reference number of the studied event. For each group of temperatures, no distinction were done between pulses acquired at different cathode biases.

Fig. 12. Averaged values of the calculations performed for $\mu_e$ at different temperatures, together with the potential function that better fit the results.

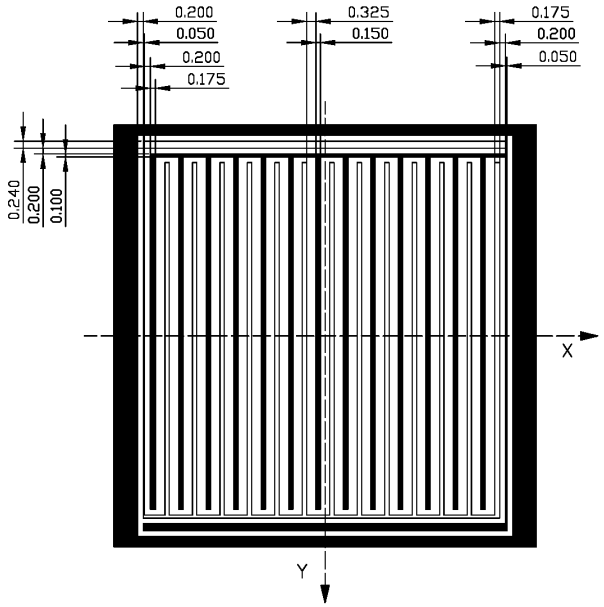


Fig. 1

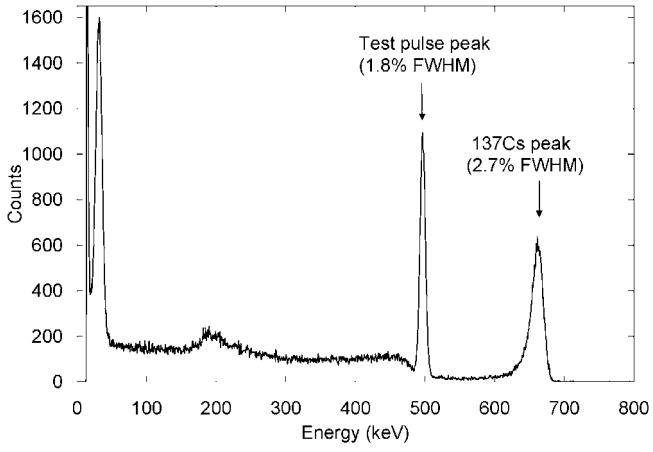


Fig. 2

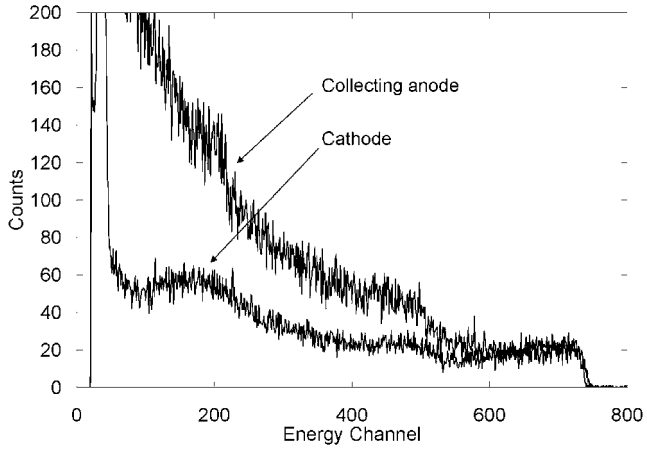


Fig. 3

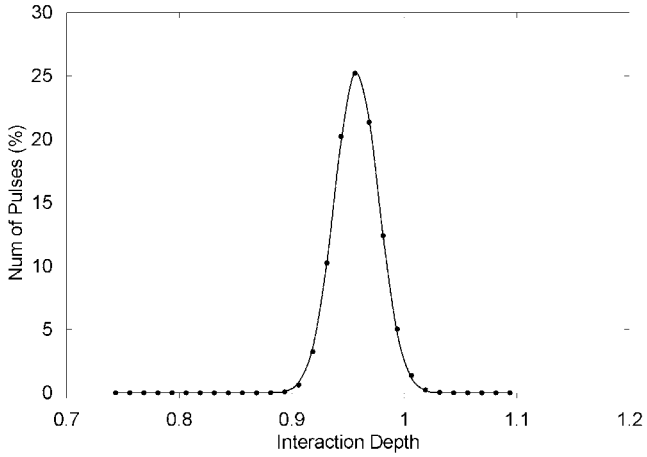


Fig. 4

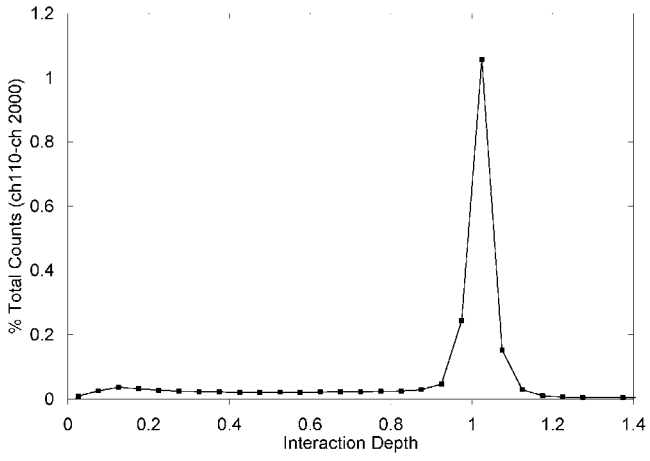


Fig. 5

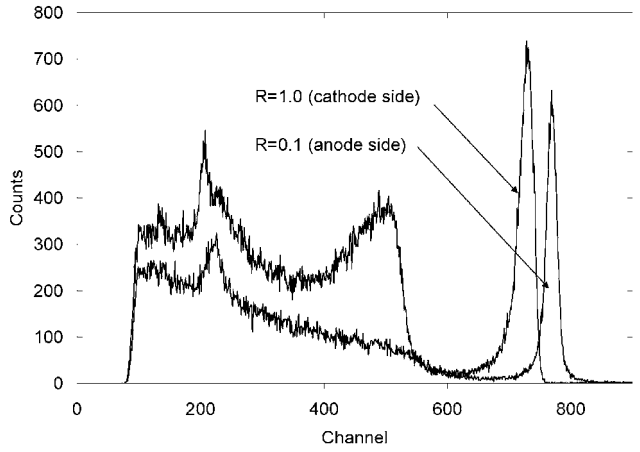


Fig. 6.

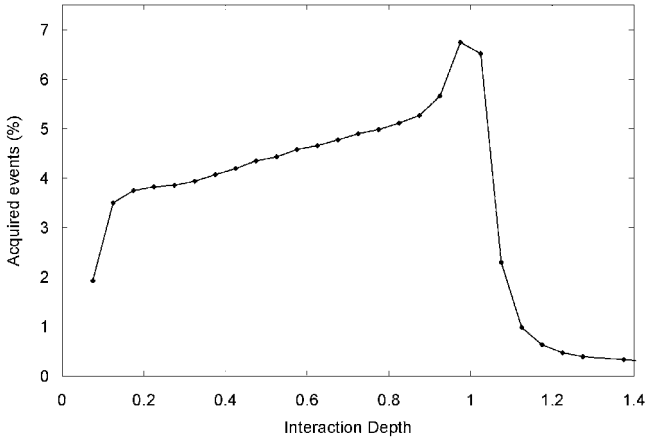


Fig. 7.a

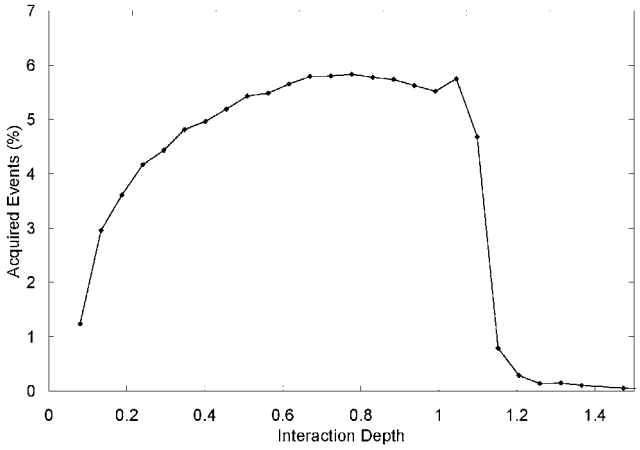


Fig. 7.b

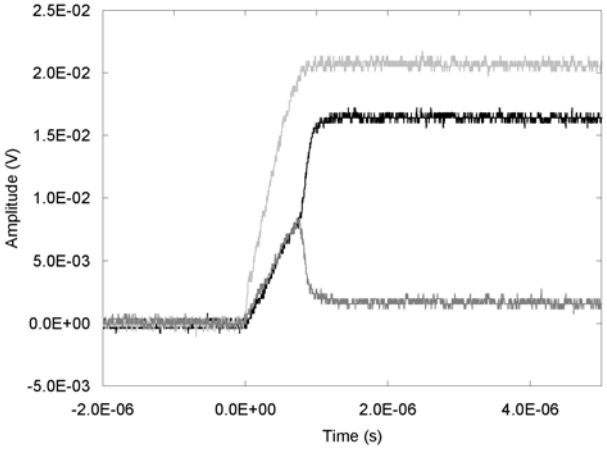


Fig. 8.a

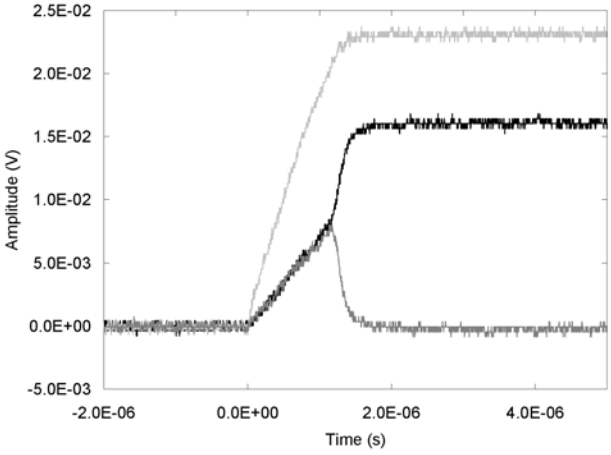


Fig. 8.b

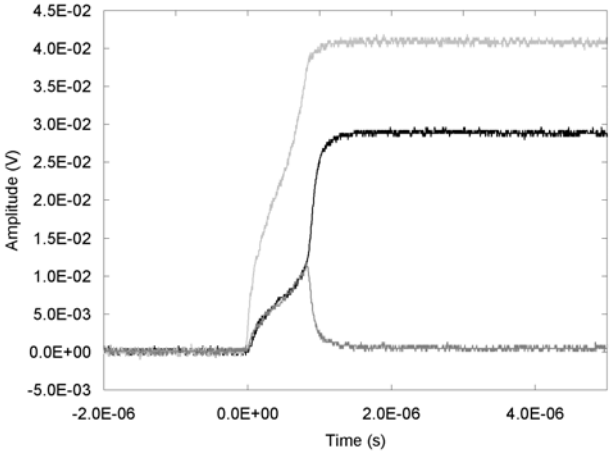


Fig. 8.c

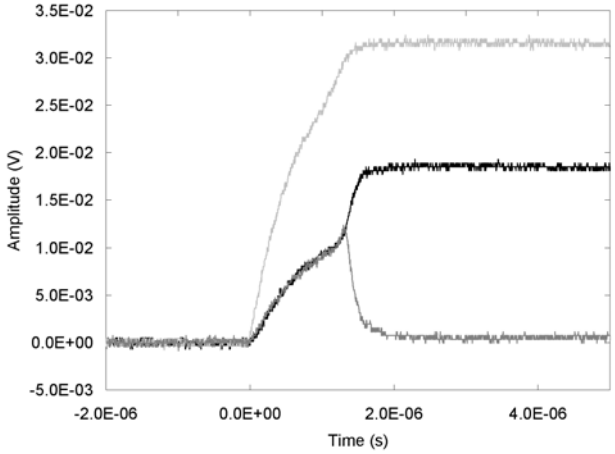


Fig. 8.d

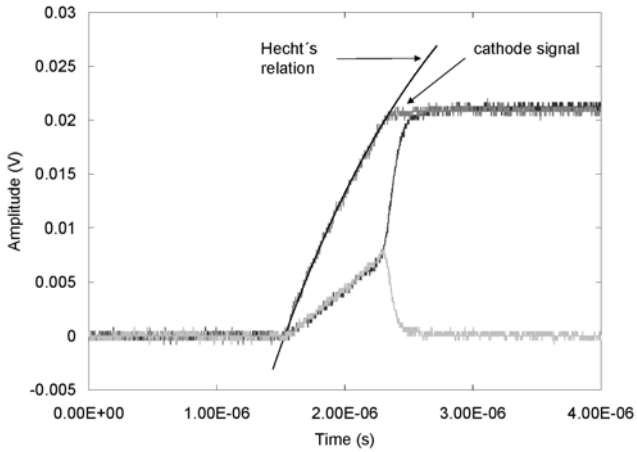


Fig. 10

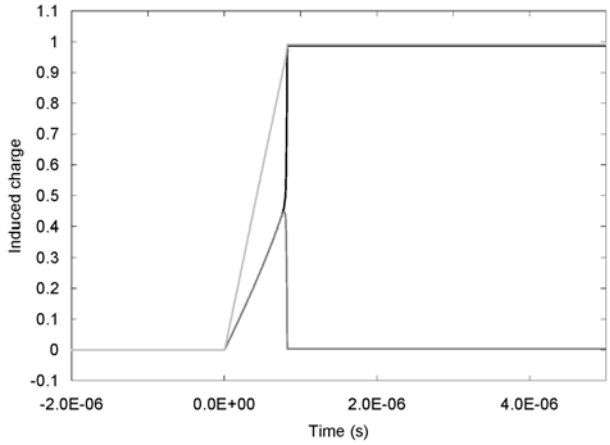


Fig. 9.a

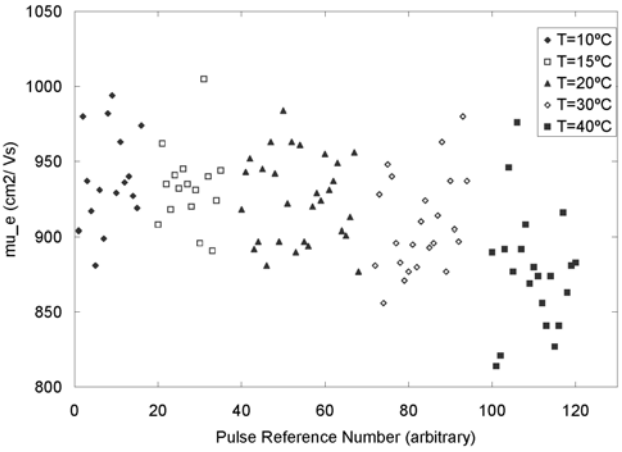


Fig. 11

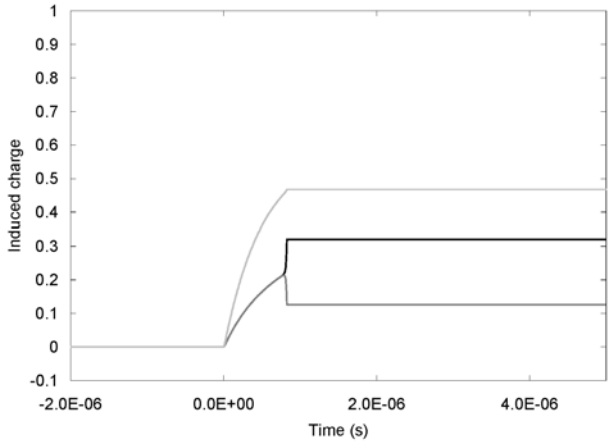


Fig. 9b

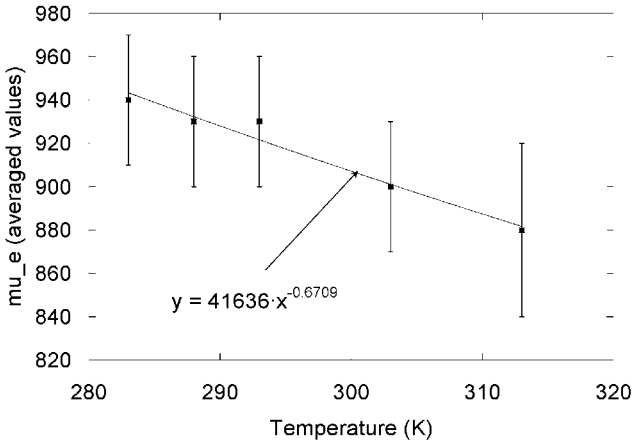


Fig. 12